



ISSN: 0067-2904

Investigation of The Characteristics of CO (1-0) Line Integrated Emission Intensity in Extragalactic Spirals

Dua'a K. A. *, M. N. Al Najm**

Department of Astronomy and Space, College of Science, University of Baghdad, Baghdad, Iraq

Received: 2/5/2021

Accepted: 6/6/2021

Abstract

This paper aims to deal with the understanding of properties of molecular gas hydrogen in extragalactic spirals sample. It is critical to make observations of CO ($J = 1-0$) line emission for spiral galaxies, particularly those with an energetic nucleus. In a compiled sample of spiral galaxies, a carbon monoxide CO (1-0) emission line can be observed. This sample of galaxies' gas kinematics and star-forming should be analyzed statistically utilizing appropriate atomic gas HI, molecular gas H_2 , infrared ($1\mu m-1000\mu m$), visual (at $\lambda_{blue-optical} = 4400\text{\AA}$), and radio spectrum (at $\nu_{radio} = 1.4$ GHz and 5 GHz) databases. STATISTICA is a software that allows us to perform this statistical analysis. The presence of a high scale of star formation activity in these galaxies is dependent linearly on the correlations between galactic luminosities. Our findings show that thermal radio luminosity and L_{FIR} are closely related to CO line emission luminosity. Further, L_{CO} and M_{H_2} have a steep linear relationship, where the slope of the regression $\log L_{CO} - \log M_{H_2}$ equals 1. The L_{CO} -SFR and L_{FIR} -SFR relationship slopes are nearly linear (slope ~ 1), with a strong partial correlation R_{CO-SFR} of 0.73 between L_{CO} -SFR and a significant correlation $R_{FIR-SFR}$ of 0.5 between L_{FIR} -SFR, according to the statistical analysis. The correlation between the rate of star formation (SFR) and hydrogen gas in spirals is significant in several fields of astrophysics. Hence, it is asserted that the important point of the current study is that there is a significant link between SFR and the actual amount of cold hydrogen gas (M_{gas}) for the simple reason that in our spiral analysis, the mean atomic cold gas amount quantity is almost 6 times greater than the molecular gaseous amount.

Keywords: spiral galaxies- star-formation; molecular - atomic gas; CO line – infrared emission; statistics.

دراسة خصائص الكثافة المتكاملة لخط انبعاث CO (1-0) في المجرات الخارجية الحلزونية

دعاء كريم عبود* ، محمد ناجي ال نجم

قسم الفلك والفضاء، كلية العلوم، جامعة بغداد ، بغداد ، العراق

الخلاصة

تهدف هذه الورقة البحثية إلى التعامل مع فهم خصائص غاز الهيدروجين الجزيئي في عينة من المجرات الخارجية الحلزونية. من الضروري إجراء ارساد لانبعثات خط أول أكسيد الكربون CO ($J = 1-0$) للمجرات الحلزونية ، خاصة تلك التي تحتوي على نوى نشطة. في عينة المجرات الحلزونية التي تم تجميعها ، يمكن ملاحظة خط انبعاث أول أكسيد الكربون CO (1-0). هذه العينة من المجرات يجب تحليل حركة الغاز وتشكيل النجوم فيها احصائياً باستعمال الغاز الذري HI ، والغاز الجزيئي H_2 ، والأشعة تحت الحمراء ضمن المدى ($1\mu m-1000\mu m$) ، والبصرية (عند الطول الموجي الأزرق $\lambda_{blue-optical} = 4400\text{\AA}$) ،

*Email.: mohalnajm@sc.uobaghdad.edu.iq

والطيف الراديوي (عند الترددات 1.4 جيجا هرتز و 5 جيجا هرتز). STATISTICA هو برنامج يسمح لنا بإجراء هذا التحليل الإحصائي. إن وجود نطاق عالٍ من نشاط تكوين النجوم في هذه المجرات يعتمد خطياً على الارتباطات بين الضيائيات في هذه المجرات. تظهر النتائج التي توصلنا إليها إلى أن الضيائية الراديوية الحرارية وتحت الحمراء البعيدة L_{FIR} مرتبطان ارتباطاً وثيقاً بضيائية خط انبعاث أول أكسيد الكربون. علاوة على ذلك، فإن L_{CO} و كتلة الغاز الجزيئي M_{H_2} لهما علاقة خطية شديدة الانحدار، حيث يساوي ميل الانحدار بينهما إلى الواحد. ووفقاً للتحليل الإحصائي وجد أن ميل العلاقة بين L_{CO} -SFR و L_{FIR} -SFR خطية تقريباً (ميل الانحدار ~ 1)، مع ارتباط معنوي قوي قدره 0.73 بين L_{CO} -SFR وارتباط جيد قدره 0.5 بين L_{FIR} -SFR. يعتبر الارتباط بين معدل النشوء النجمي (SFR) وغاز الهيدروجين في المجرات الحلزونية مهماً في العديد من مجالات الفيزياء الفلكية. لذلك، تم التأكيد على النقطة المهمة في الدراسة الحالية وهي أن هناك ارتباطاً كبيراً بين SFR والكمية الكلية الفعلية من غاز الهيدروجين البارد (M_{gas}) لسبب بسيط هو أنه في تحليلنا للمجرات الحلزونية، وجد أن متوسط كمية الغاز البارد الذري تقريباً 6 مرات أكبر من الكمية الغازية الجزيئية.

1. Introduction

Extragalactic spirals have radio characteristics that can be observed in spectrum of radio region including spectral lines of hydrogen in addition, to ordinary molecules, like carbon monoxide spectroscopy, since the optical spiral arms are circumscribed by regions that generate stars [1]. The primary condensation and breakup of giant molecular clouds to thick accretion a disk including molecular clouds, that molecular interstellar medium plays an important part in star formation. So, the total mass of molecular gas in a galaxy is an important factor in determining star formation [2]. Even though, H_2 presents up at least 99 % of the molecular gas, it is difficult to detect directly in most of the molecular medium due to the absence of a stable dipole moment as well as its cold temperature, which is below the excited energy. As a consequence, observing the molecular gas is reliant on other molecules, especially CO, which is easily visible even in the thinnest molecular gas. To study interstellar molecular gas, the CO emission lines, especially the transition $J = 1-0$ at $\nu_{CO(1-0)} = 115$ GHz, can be compared to the 21 cm line. Carbon monoxide is the simplest molecule present in each molecular dust of the Milky Way, including any galaxy at any redshift, and it is utilized to calculate the masses of molecular gas systematically [2].

The molecular hydrogen is highly intertwined with atomic hydrogen, and the total amount of gas $M_{H_2}+M_{HI}$ is the most significant quantity for the evolution and formation of spiral galaxies including, in some way, star formation. Atomic gas (HI) and molecular gas are inextricably connected. Due to the continuous exchange between HI and H_2 , the gas must be fully studied, as well as its dynamics, transport characteristics, including interchanges alongside the intergalactic medium and interior regions, and concentration processes that lead to star formation and the effect of reactions on the gas [2]. Far-infrared luminosities of $L_{FIR} \approx 10^{13} L_{\odot}$ are observed in the majority of CO-detected sources. In local ultra-luminous infrared galaxies (ULIRGs), there exist a trend of higher values for the ratio of Far-infrared luminosity to CO radiance compared to the association between CO and FIR luminosities [3]. Interstellar gas must be studied at galactic measures to understand the composition and dynamics of galaxies, as well as how stars form. Apart from interstellar dust extinction, the bulk of the interstellar medium is inaccessible to optical astronomy due to the absence of emission at low temperatures, a lack of adequate visual absorption bands, and absorption line obscuring caused by massive dust extinction [4].

Several studies focused on galaxies were being conducted to investigate the properties of CO line emission in galactic centers and disks. Using single-dish extragalactic spectra synthetic emission, Lavezzi & Dickey (1997) investigated disk resolution testers, calculated distributions of gas density, and opacity to assess if CO line widths for use in the Tully-Fisher relationship are correct. Researchers used an HI of 21 cm line, confined gas density

distributions, and opacity on extragalactic spirals spectra instead of an HI of 21 cm line to view if CO line widths were appropriate for use in the Tully-Fisher relation [5]. Boselli et al. (2002) analyzed the relationship between the H_2 to CO conversion factor and galactic parameters including UV, metallicity, and blue optical and near-infrared luminosities. The relationship between star formation activity and total mass of gas $M_{H_2} + M_{HI}$ has been discovered, with the understandable reason that for spirals, the mean M_{H_2}/M_{HI} effect is nearly constant. [6].

In the following study [7], the researchers concentrated on knowledge of the large mass of H_2 traced by CO millimeter emission in regular molecular clouds. In the external galactic disk, an even greater mass of H_2 may be obscured as incredibly cold hydrogen. Since the first extragalactic CO surveys, there has been a clear correlation between CO flux energy (I_{CO}) and both radio continuum and Far-infrared luminosities. Making this association quantitative with SFR, except for non-starburst galaxies, poses many challenges, including the most critical case of spiral galaxies as exhibited in [8]. CO line intensity studies of molecular gas in galaxies bars, as demonstrated by Jogee et al. (2005), are critical for understanding their structure and dynamics, as well as their effect on the rate of star formation in the nuclear surroundings [9]. The author Al Najm (2020) discussed the physical properties of a sample of 65 CO(J=1-0) line spectra of extragalactic (normal and active galaxies), which are characterized by the effectiveness of stellar evolution. These galaxies have a large molecular mass as well as a large star formation activity per unit “mass”, according to the findings [10]. This paper is structured as ensues: in Parts 2 and 3, we explain the sample and also the physical parameters derived from spectral information and used in the study. Part 4 delves into the results of the analyses. A summary is given in the final part.

2. Data Collection for Sample Observations

NASA /IPAC Extragalactic Database (NED) mission archives website was used to extract some parameters such as infrared fluxes at near, medium, and far beams F12, F25, F60, & F100 in the unit (Jy) within the wavelengths (12, 25, 60 and 100) μm , radio continuum flux at 1.4 GHz ($\lambda_{radio}=21$ cm) & 5 GHz ($\lambda_{radio}=6$ cm) and redshift (z). French website Lyon-Meudon Extragalactic Database (hyperLeda) was used to extract some parameters such as the magnitude of neutral hydrogen (HI) line at the 21 cm, the morphological type of galaxies, the angular diameters, and blue apparent magnitude (mBtc) galactic extinction correction. The literature papers [11,12,13] were used to collect the flux-limited at the carbon monoxide line transitions ICO (12CO J=0-1) radiation, as well as extracted half-power beam width (θ_{HPBW} in-unit arcsec) for radio telescopes were detectable at rest frequency $\nu_{rest} \approx 115.27$ GHz ($\lambda_{rest} = 2.6086$ mm): IRAM (at 30 m), BTL (at 7 m), FCRAO (at 14 m), MRT (at 2048 m), NRAO (at 12 m), NRAO (at 45 m), SEST (at 15 m). The total number of 12CO(1-0) line detected spiral galaxies is 140. The physical parameters (name galaxy, the morphology of spiral galaxies, m21, z, mBtc, ICO(J=1-0), θ_{HPBW} , F12, F25, F60, F100, and radio fluxes at $\nu=1.4$ GHz & $\nu=5$ GHz) of any chosen galaxy are noted in Table(1).

3. The Computed Parameterization

Carbon monoxide CO is the most common compound in the interstellar medium. A rotating molecule of carbon monoxide, for example, emits dipole radiation at the frequency of its rotation, as follow [14]:

$$\nu \approx \frac{v_r}{2\pi a} \dots \dots \dots (1)$$

where v_r and a is the circumrotation speed of the molecule and its length (C separator and O atoms). The lowest frequency of the rotational transition from $J = 1$ to the ground level $J = 0$ for the CO line intensity is approximately $\nu_{J=1-0} = 115$ GHz or $\lambda_{J=1-0} = 2.6$ mm [14]. The following variables were computed separately:

1-To calculate the total H_2 mass (M_{H_2}), we began to calculate the CO radiance by combining the CO(1-0) line intensity across the speed profile. The luminance of the CO line is generally displayed in units of $K.km/s.pc^2$ as a result of the reference integrated velocity illumination temperature ($T_b \Delta v$) and the source area $\Omega_s D_A^2$, where Ω_s is the solid angle that the source takes. The intensity of the observed integral line $I_{CO} = \int T_{mb} dv$, which decreases with redshift, measures the brightness weak temperature of the beam. If so, it is referred to as the main temperature beam T_{mb} , which is roughly equal to the cloud temperature T_b brightness [15, 16]:

$$T_b \Delta v \Omega_s = 23.5 I_{CO} \Omega_{sb} (1+z) \dots \dots \dots (2)$$

where Ω_{sb} is the source's solid angle when coiled with the telescope beam. Therefore, the CO(1-0) line intensity luminosity is given by

$$L_{CO} = T_b \Delta v \Omega_s D_A^2 \dots \dots \dots (3)$$

The luminosity distance D in the unit (Mpc) to the moving source by the redshift (z) can be viewed from the following [15, 16]:

$$D = D_A (1 + z)^2 \dots \dots \dots (4)$$

where D_A is the angular size distance. According to the NASA /IPAC Extragalactic Database site (NED), we adopt a Hubble constant of $H_0 = 100 h \text{ km s}^{-1} / \text{Mpc}$ with uncertainty in the Hubble constant scale $h = 0.678 \pm 5$ and cosmological parameters $\Omega_{\text{matter}} = 0.308$ and $\Omega_{\text{vacuum}} = 0.692$. In cosmology, the luminosity distance and the angular size have been calculated using the website (<http://www.astro.ucla.edu/~wright/CosmoCalc.html>). By substituting equations (2 & 4) in the expression equation (3), then, the CO line luminosity (L_{CO}) for a source takes the form:

$$L_{CO} = 23.5 I_{CO} \Omega_{sb} \frac{D^2}{(1+z)^3} \quad \text{is measured in unit } K. \text{ km s}^{-1}. pc^2 \dots \dots \dots (5)$$

where I_{CO} is the line intensity by unit $K \text{ km s}^{-1}$ and beams solid angle of radio telescope $\Omega_{sb} \approx 1.13 \theta_{HPBW}^2$

Hence, equation (5) can be rewritten as follows:

$$L_{CO} = 26.55 I_{CO} \theta_{HPBW}^2 \frac{D^2}{(1+z)^3} \dots \dots \dots (6)$$

or the equation (6) can be written in the form of a logarithm:

$$\text{Log } L_{CO} = 1.424 + \text{Log } I_{CO} + 2 \text{Log } \theta_{HPBW} + 2 \text{Log } D - 3 \text{Log } (1 + z) \dots \dots \dots (7)$$

2- Molecular hydrogen gas content (M_{H_2}) in unit solar mass (M_\odot) is estimated from the $^{12}\text{CO}(J=1-0)$ integrated intensity using the following equation [17]:

$$M_{H_2} = 97.8 \theta_{HPBW}^2 I_{CO} D^2 \dots \dots \dots (8)$$

A logarithmic scale of M_{H_2} in the unit (M_\odot) can be computed as ensues:

$$\text{Log } M_{H_2} (M_\odot) = 1.99 + 2 \text{Log } \theta_{HPBW} + \text{Log } I_{CO} + 2 \text{Log } D \dots \dots \dots (9)$$

3- Infrared Luminosity L_{IR} was determined utilizing the usual definitions of the luminosity distance D [18]:

$$L_{IR} = 4\pi D^2 \int_{1\mu m}^{1000\mu m} F_\lambda d\lambda, \quad \text{where } F_\lambda \text{ is flux density} \dots \dots \dots (10)$$

The infrared luminosity L_{IR} between bands $1 \mu m$ to $1000 \mu m$ of galaxies has been computed from the IRAS flux densities according to fluxes F_λ at 12, 25, 60, and $100 \mu m$ [19 & 20]

$$\text{Log } L_{IR} (L_\odot) = 5.5378 + 2 \text{Log } D + [12.66 F_{12} + 5.00 F_{25} + 2.55 F_{60} + 1.01 F_{100}] \dots \dots \dots (11)$$

Where F_{12} , F_{25} , F_{60} , and F_{100} are the relevant IRAS apparent flux densities for a source expressed in the Jansky unit (Jy), where $1 \text{ Jy} = 10^{-26} \text{ W/m}^2 \text{ Hz}$

4- The luminosity of 60 microns of the IRAS - $60 \mu m$ range in solar luminosity is described as follows [21]:

$$\text{Log } L_{60\mu m} (L_\odot) = 6.014 + 2 \text{Log } D + \text{Log } F_{60} \dots \dots \dots (12)$$

where F_{60} means IRAS $60 \mu m$ band flux intensity in Jy.

5-The Far-infrared luminosity (L_{FIR}) in solar luminosity (L_{\odot}) at bands IRAS 60 μm and IRAS 100 μm is given by[22] :

$$L_{FIR}(L_{\odot}) = L_{60\mu m} + L_{60\mu m} \left(\frac{F_{100}}{2.58 F_{60}} \right) \dots \dots \dots (13)$$

6- The radio luminosity at a frequency 1.4GHz was computed adopting the next relation [22]:

$$\text{Log } L_{1.4\text{GHz}}(W Hz^{-1}) = 20.08 + 2\text{Log } D + \text{Log } F_{1.4} \dots \dots \dots (14)$$

Here, $F_{1.4}$ is the radio extended flux density in units of Jy at the emitted rest frequency $\nu_{\text{radio}} = 1.4 \text{ GHz}$ or ($\lambda_{\text{radio}} = 21 \text{ cm}$) arising from hyperfine spin relaxation.

7- The total mass of neutral hydrogen gas (HI) in solar mass (M_{\odot}) was measured using the standard method, using a magnitude of 21 cm (m_{21}), and since HI is visually light on galactic estimates, the strength of the HI line is mass proportional [23, 24]

$$MHI(M_{\odot}) = 2.36 \times 10^5 x \left(\frac{D}{1 \text{ Mpc}} \right)^2 \int S_{HI,v} dv \dots \dots \dots (15)$$

The raw fluxes $S_{HI} = \int S_{HI,v} dv$ is the density of the HI line integrated into Jy Km/s collected in the literature is converted into a logarithmic scale using m_{21} apparent magnitudes defined as [25]:

$$\text{Log } S_{HI} = -0.4(m_{21} - 15.84) + 0.626 \dots \dots \dots (16)$$

or

$$S_{HI} = 10^{-0.4(m_{21}-15.84)+0.626} \dots \dots \dots (17)$$

8- Logarithm of the blue visual luminosity (L_B) in solar units at the blue wavelength 4400Å°, computed using [26, 27]

$$\text{Log } L_B(L_{\odot}) = 12.164 + 2 \text{Log } D - 0.4 m_{Btc} \dots \dots \dots (18)$$

m_{Btc} is the total value of the corrected blue color-magnitude for galactic and endogenous absorption.

9- The central radio continuum luminosity at frequency $\nu = 5 \text{ GHz}$ or wavelength $\lambda = 6 \text{ cm}$ can be written as [26]:

$$\text{Log } L_{6cm}(L_{\odot}) = 17.078 + 2 \text{Log } D_{Mpc} + \text{Log } F_{6cm} \dots \dots \dots (19)$$

10- The dust mass in galaxies (M_{dust}) is calculated from the temperature of the dust, T_{dust} , which is inferred from the flux densities at the emission of 60 μm and 100 μm from the black body. Considering that the dust radiation attends the emissivity law $F_{\nu} \propto \lambda^{-1}$, the M_{dust} almost designated as [17, 28]:

$$M_{\text{dust}}(M_{\odot}) = 4.5 F_{100\mu m} D^2 (e^{2.94 * (F_{100}/F_{60})^{0.4}} - 1) \dots \dots \dots (20)$$

Dust temperature T_{dust} can be calculated according to IRAS flow densities of 60 micrometers and 100 micrometers [29]:

$$T_{\text{dust}} = -(1+z) \left[\frac{82}{\ln(0.3 F_{60\mu m} / F_{100\mu m})} - 0.5 \right] \text{ in unit } K^0 \dots \dots \dots (21)$$

11- Total cold hydrogen gas masses M_{gas} were computed by combining the above-mentioned molecular and atomic gas mass with 30% helium (He) contribution [30]:

$$M_{\text{gas}} = (MHI + MH_2) / \beta \dots \dots \dots (22)$$

where $\beta \approx 0.74$ is the standard hydrogen part of neutral gas, and the remainder is helium and a small fraction of heavier elements[24]. So the equation (21) becomes as follows:

$$M_{\text{gas}} (\text{in unit } M_{\odot}) = 1.3 (MHI + MH_2) \dots \dots \dots (23)$$

12- Star formation rate SFR in-unit $M_{\odot} \text{ yr}^{-1}$ is estimated in Far-infrared energy radiation from the relationship[10]:

$$SFR(M_{\odot} \text{ yr}^{-1}) = 1.7 \times 10^{-10} L_{FIR} \dots \dots \dots (24)$$

4. Statistical Calculation Results and Discussion

We utilized a statistical software program (statistic-win-program) to see if there is a correlation between several variables in this article. The statistical program is commonly used

to process and evaluate various relationships between variables, as well as to assess if there is regression strength between the characteristics of the two variables. The values of the linear partial correlation coefficient (R) are in the range $[-1, +1]$. The two components are completely associated if the regression value is ± 1 . Even so, there is a weak regression correlation between the two components when the measurement of regression correlation (R) is zero or close to zero [10, 31-34]. Due to Malmquist bias, both correlation coefficients and confidence levels have been adjusted for artificial reliance on parameters from galaxies distances in this work. Molecular hydrogen and neutral hydrogen are the most common cold interstellar medium ISM types. Carbon monoxide observations have allowed identifying the molecular gaseous hydrogen emission in detail to other observations at different frequencies ranging from ultraviolet-optical-infrared to radio bands.

According to statistical regression techniques for the analysis of (140) extragalactic spirals, the average value of CO(1-0) luminosity with a standard error is equivalent to $\langle \text{Log } L_{\text{CO}} \rangle = 8.10 \pm 0.073$ ($L_{\text{CO}} = 12.6 \times 10^7 \text{ K. kms}^{-1} \cdot \text{pc}^2$) with a minimum and maximum value ranging between $L_{\text{CO min.}} \sim 2.73 \times 10^5 \text{ K. km/s.pc}^2$ to $L_{\text{CO max.}} \sim 1.25 \times 10^{10} \text{ K. km/s.pc}^2$, while a mean value of IR-infrared (1-1000) μm to Far-infrared around 100 μm luminosity can be evaluated $\langle L_{\text{FIR}} (L_{\odot}) \rangle \approx 8.5 \times 10^9 \pm 0.067$ with $L_{\text{FIR min.}} = 10^7$ to $L_{\text{FIR max.}} \approx 3 \times 10^{12} L_{\odot}$ for the warm dust of temperature about $\langle T_{\text{dust}} \rangle = 42 \pm 0.925 \text{ K}^0$. Since the dependence of the temperature dust on the CO (1-0) line-infrared emissions as shown as Figure (1a) existence a positive relationship between ($\text{Log } L_{\text{FIR}}$, $\text{Log } L_{\text{CO}}$, and T_{dust}) with a flat slope \leq of 0.5 for relation $\text{Log } L_{\text{FIR}} - T_{\text{dust}}$ and $\text{Log } L_{\text{CO}} - T_{\text{dust}}$. We adopted the following equation for linear fit regression $Y = ax + b$, where (a) is just the slope of linear regression, and (b) is the y-axis intercept, the most appropriate suitable fitting expression of linear regression is found using an acceptable standard error, which is described as:

$$\text{Log } L_{\text{CO}} = (0.16 \mp 0.048) T_{\text{dust}} + (4.89 \mp 0.24) \dots \dots \dots (25); \text{ and} \\ \text{Log } L_{\text{FIR}} = (0.31 \mp 0.06) T_{\text{dust}} + (7.05 \mp 0.25)$$

and we have seen that there is a partial correlation coefficient equal to ($R_{\text{FIR-Tdust}} = 0.42$, $R_{\text{CO-Tdust}} \approx 0.3$) in this relationship. Figure 1a exhibits the relationship between CO line -FIR infrared luminosity and dust temperature for the extragalactic spiral in this study. The correlation between L_{CO} and T_{dust} is slightly weaker than that between L_{FIR} and T_{dust} . Besides, results pointed also to a good positive relationship between $L_{\text{CO-LIR}}$ and $L_{\text{CO-LFIR}}$ ($\text{Log } L_{\text{CO}} \propto \text{Log } L_{\text{IR}}^{0.62 \pm 0.056} \propto \text{Log } L_{\text{FIR}}^{0.65 \pm 0.053}$) with a strong correlation is equal to $R \sim 0.7$ and a very higher probability level of chance correlation $P \leq 10^{-7}$ (see Figures 1b & 1c). The physical meaning of these correlations can be clarified by the amount of interstellar medium gas in a molecular form (CO) that significantly increases with IR-FIR luminosities, according to our results. These galaxies show extremely high infrared detection lines from the line intensity of carbon monoxide CO as shown in a ratio $L_{\text{FIR}}/L_{\text{CO}} = 1.84$ computed from our results, and also the warm dust element cohabits with the molecular layer formed of warm clouds ($\langle T_{\text{dust}} \rangle \approx 40 \text{ K}$) at the actual scale, indicates that the warm dust element emits in the near-infrared range, with a peak of about 100 μm , since the dependence of the temperature dust on the infrared emission. The ultraviolet (UV) and optical emission absorbed from OB stars are the sources of the FIR -infrared emission's spectral energy. The broad range of observed radiation indicates that the distance measured will not influence the association between FIR and CO luminosities, showing an excess of far-infrared emission. It appears to us that the outcomes of our work here are in agreement with those of previous literature articles such as [20, 10, and 16] on the strong link between LCO-LIR and LCO-LFIR

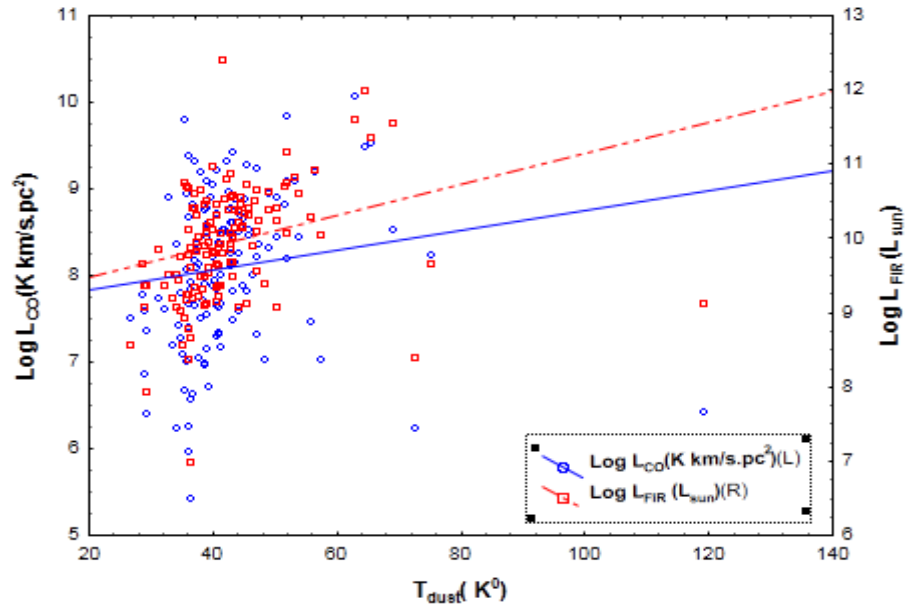


Figure 1- (a) Two commons of the relationship between CO line and FIR-infrared luminosity versus T_{dust} . The straight blue line represents fitting for all results for L_{CO} and the dashed red lines describe fitting for all database L_{FIR} vs. T_{dust}

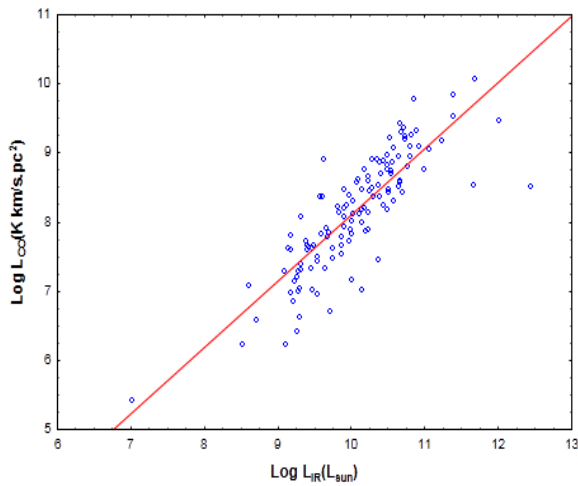


Figure 1- (b) The relationship between $(Log L_{CO})$ and $(Log L_{IR})$.

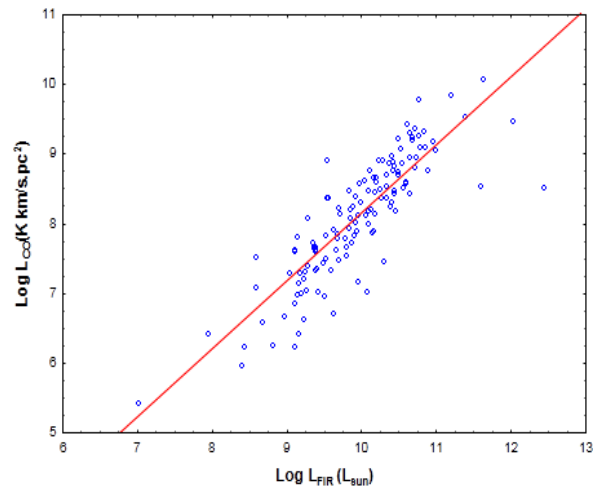


Figure 1- (c) The relationship between $(Log L_{CO})$ and $(Log L_{FIR})$.

The relationship between CO line emission luminosity and $L_{1.4}$, L_{6cm} , L_B optical blue luminosities respectively has been inferred in the present study. It is clear from Figures 2a, 2b and 2c) that there is a positive correlation between L_{CO} and $L_{1.4}$ ($R \approx 0.5$), however, there seems to be a statistically significant correlation coefficient between L_{CO} and L_{6cm} , L_B equals to $R \sim 0.7$, in addition to a very significant level of confidence $P \leq 10^{-7}$, and we noticed differences in slopes between $(Log L_{CO} \propto Log L_{1.4}^{0.58 \pm 0.05})$, $(Log L_{CO} \propto Log L_{6cm}^{0.61 \pm 0.09})$, as well $(Log L_{CO} \propto Log L_B^{0.39 \pm 0.05})$. We found a tight linear relation between CO(J=1-0) line emission and radio continuum with either L_{CO} - L_{6cm} or L_{CO} - $L_{1.4GHz}$ and the CO(1-0) line emission of spiral galaxies is also related to the blue optical emission (L_B). It can be understood in these types of galaxies, as well as an abundance of gases that pervade the entire galaxy. An ionized gas H_α at line $\lambda = 6$ cm can emit a heavy radio and thermal emission. This implies that these extragalactic spirals with bright CO line densities or the radio thermal continuum have more atomic and molecular gas, regardless of form. It's interesting to note

that the range of optical blue brightness difference in our sample is rather limited, or maybe suggesting that the correlation between CO (1-0) line emission and radio continuum seems to be more essential.

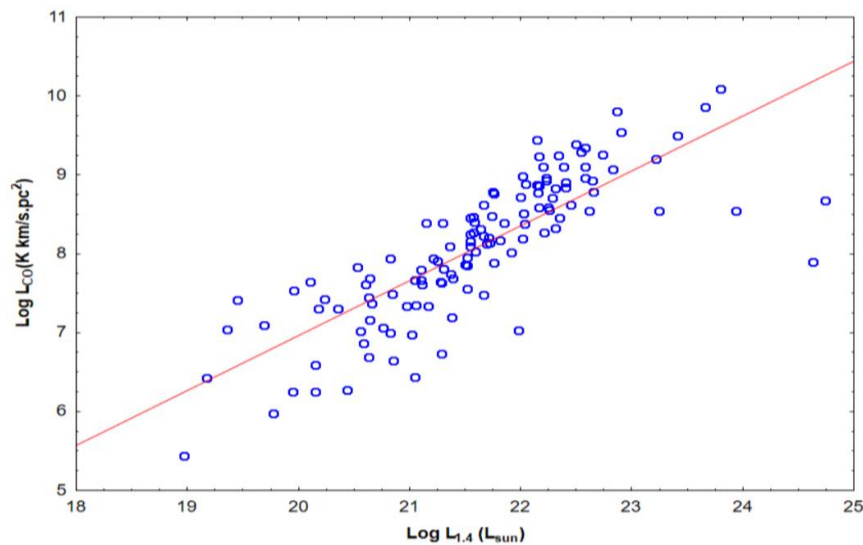


Figure 2- (a) The relationship between ($\text{Log } L_{\text{CO}}$) and ($\text{Log } L_{1.4}$) luminosity.

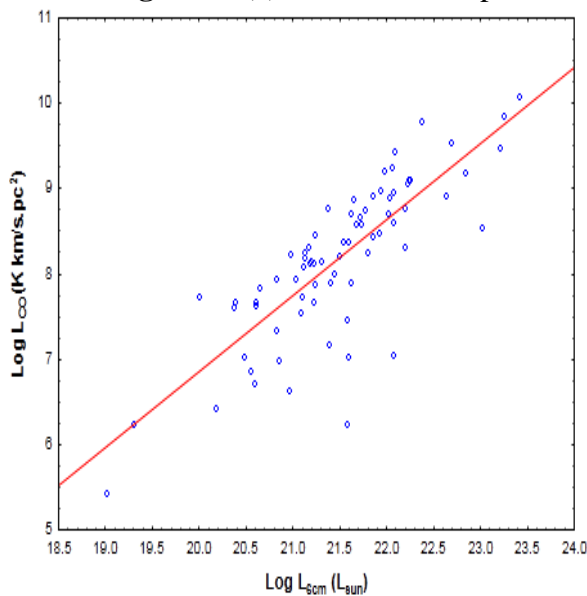


Figure 2- (b) The relationship between ($\text{Log } L_{\text{CO}}$) and ($\text{Log } L_{6\text{cm}}$) .

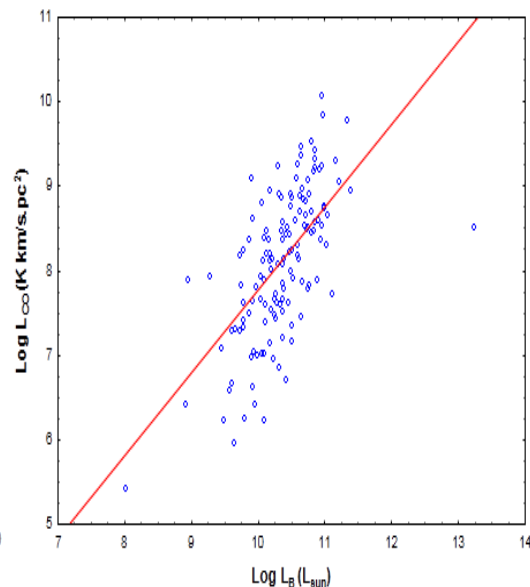


Figure 2- (c) The relationship between ($\text{Log } L_{\text{CO}}$) and ($\text{Log } L_{\text{B}}$) .

We estimated the mean values of atomic cold hydrogen gas (MHI), molecular cold gas content (MH₂), and dust mass (M_{dust}) for our galaxies. Consequently, to our sample of the extragalactic spirals the mean values with a standard error of $\text{Log MHI}=9.43\pm0.059$, $\text{Log MH}_2=8.68\pm0.074$, and $\text{Log M}_{\text{dust}}=6.46\pm0.069$ respectively. It is essential to see that for all morphological types of spiral galaxies, the hydrogen HI content is always greater than that of the content hydrogen H₂, the cold atomic gas content increases approximately by a factor of 6 to the molecular mass value of the gas in spiral galaxies ($< \text{MHI} / \text{MH}_2 > \approx 6$). As we have previously indicated that the molecular gas mass is associated with the carbon monoxide gas CO line, furthermore, the CO(J=1–0) spectroscopic database was used to measure the molecular hydrogen amounts of spiral galaxies, accordingly, the neutral gas HI surface area in most morphology spiral galaxies is larger than the CO line amplitude. The CO radiation is

focused in the interior some kiloparsecs whereas, a natural gas distribution indicates more depression in the galaxy's center. Besides that, for HI cold gas observations, the superposition of independent clouds in the emission region is more expensive than toward molecular gas CO observations. Our results calculated here are largely in agreement with those of the literature [26]. The average value of the ratios of M_{H_2}/M_{dust} was evaluated in this survey, for our types galaxies having $\Delta \text{Log} (M_{H_2}/M_{dust})$ designated as $< \text{Log} M_{H_2} > - < \text{Log} M_{dust} >$ equals the mean value 2.21 ± 0.047 , this means that the molecular gas mass M_{H_2} is about ~ 160 times larger from dust mass M_{dust} of those galaxies. The method for calculating dust mass utilizing Far-infrared flux at $60 \mu\text{m}$ and $100 \mu\text{m}$, and the molecular gas mass to dust mass ratio seems to be overestimated. This indicates that the dust components contain most of the cold dust and a fraction of warm dust. Two dust components, warm and cold dust, have been proposed as explanations for the difference in the gas-to-dust masses ratio. Cold ($T_{dust}=10\text{-}20 \text{ K}^0$) dust associated with quiescent molecular clouds and warm ($T_{dust}=30\text{-}60 \text{ K}^0$) dust associated with a star-forming activity. Our interpretation of this finding is identical to what was mentioned in the investigation article [28].

As shown in Figures (3a, 3b & 3c), the relation between atomic and molecular gas-to-dust content and CO line luminosity has also been discussed, and we discovered differences in the slopes between them. In Figure.3a we have noticed that there is a very tight linear relationship between L_{CO} and M_{H_2} , the slope of $\text{Log } L_{CO} - \text{Log } M_{H_2}$ equal to unity (slope ≈ 1), with a very strong correlation coefficient corresponding to 1 ($R_{CO-MH_2}=1$) and a very high probability of relationship $P \leq 10^{-7}$. In contrast, it is evident from Figure (3b) that there is a weak correlation between L_{CO} and M_{HI} , the slope of the relationship between CO line emission and atomic cold gas is not linear but rather flat (slope ~ 0.3) and a weak correlation $R_{CO-MHI} \sim 0.35$, as for the relation $L_{CO} - M_{dust}$ there is a good correlation between them ($R_{CO-Mdust} \sim 0.64$), then the linear regression slope towards one as given as in Figure (3c). The very strong linear association potential between L_{CO} with M_{H_2} distinct in these types of galaxies indicates that the molecular gas is more abundant due to its wide diffusion, due to the molecular gas's effectiveness in the M_{H_2} regions. Intergalactic gas emits a lot of ^{12}CO ($J=1\text{-}0$) lines, which is dominated by the molecular gas H_2 . As a result, gas content-to dust mass to CO line luminosity relationships in these spiral galaxies are varied and complex, dependent on a range of internal and external variables including the atmosphere, brightness, dynamics, structure, and star formation activity. Observing emission from CO line rotational transitions is the most popular form of pursuing intergalactic molecular clouds, which are almost completely made up of molecular hydrogen. All interstellar clouds are mostly made up of molecular hydrogen instead of atomic hydrogen. The transition from atomic hydrogen to molecular hydrogen appears at a medium interstellar surface region, suggesting that whole massive clouds are molecular gas. Molecular gas clouds provide the materials for star-forming and are an important part of galaxies' evolution. Interstellar dust, on the other hand, is responsible for the massive CO emission to infrared luminosity seen in an extragalactic spiral, and all dense, dusty particles may be considered molecular.

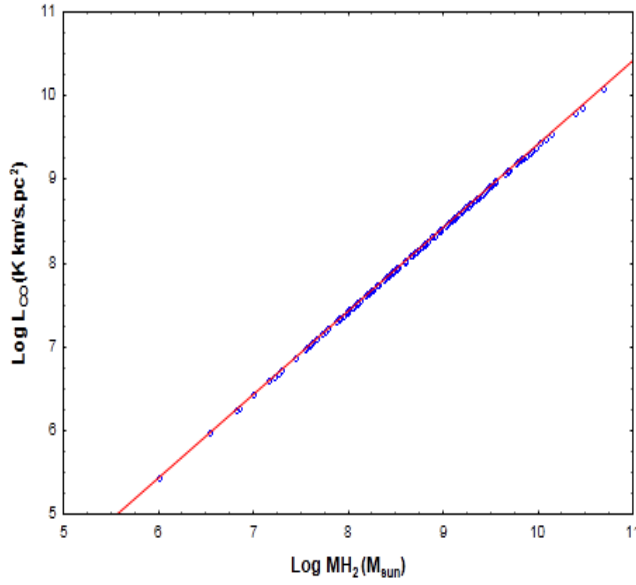


Figure 3- (b) The relationship between

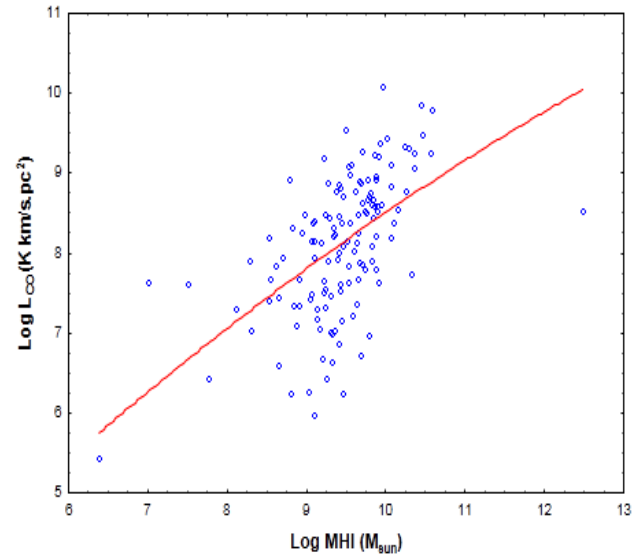


Figure 3- (a) The relationship between (Log L_{CO}) and (Log MHI). (Log L_{CO}) and (Log MH₂)

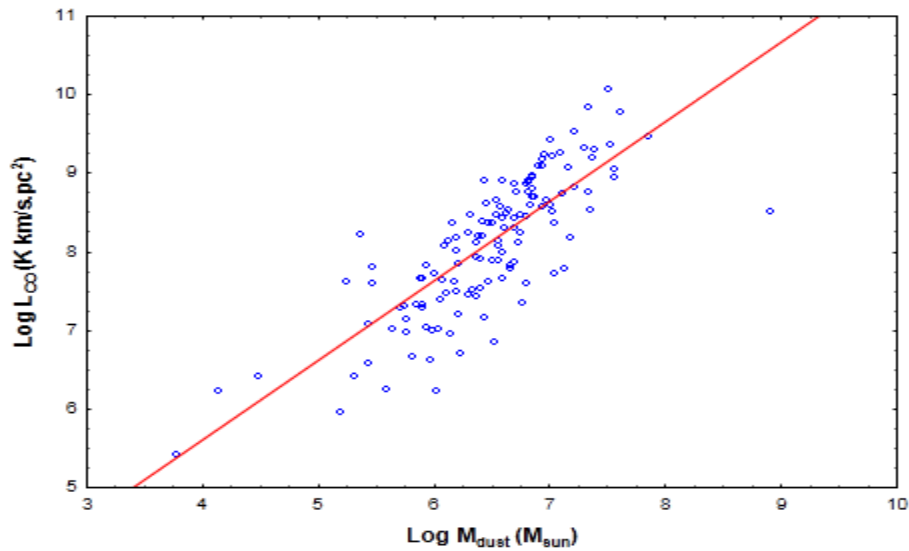


Figure 3- (c) The relationship between (Log L_{CO}) and (Log M_{dust})

It is seen from our work, the average value of star formation rate $\langle \text{SFR} \rangle = 8.98 \pm 3.73$ with lower and upper quartile values is located between $0.41 \text{ M}_\odot \text{ yr}^{-1}$ and $4.58 \text{ M}_\odot \text{ yr}^{-1}$, regardless of the morphological type, in the most reliable SFR measurements. It has been estimated that there is a strong relationship between the star formation indicator rate SFR and both the far-infrared and CO luminosities. We noticed that slopes of the relationships $L_{\text{CO}}\text{-SFR}$ and $L_{\text{FIR}}\text{-SFR}$ are approximately linear ~ 1 with a strong partial correlation coefficient $R_{\text{CO-SFR}} \approx 0.73$ between $L_{\text{CO}}\text{-SFR}$, whereas a clear correlation $R_{\text{FIR-SFR}} \approx 0.5$ between $L_{\text{FIR}}\text{-SFR}$ and probability of occurrence correlation is very high ($P \leq 10^{-7}$) as illustrated in Figure 4a (left panel). Star formation rate seems to be the product of a complex interstellar medium mechanism that leads to the separation and collapse of stellar scale clusters. The majority of the steps indicate energy density at which the interstellar gas must be molecular gas including

the extragalactic spirals. There should be strong significant relationships between the amount of molecular gas CO and star formation activity higher than the amount of Far-infrared radiation and spiral galaxies' SFR on all scales. For note, a portion of the Far-infrared radiation in some spiral galaxies can occur in the distributed atomic layer, making star formation regions irrelevant.

In Figure 4b (right panel/ solid blue line), we analyze the accumulated correlations of a range of variables such as the total mass of cold gas ($M_{\text{HI}}+M_{\text{H}_2}$), and ratio $L_{\text{FIR}}/L_{\text{B}}$ with star formation indicator. It is explicit that the main finding of the current study is that there is a significant relationship between SFR and the total amount of cold gas M_{gas} . The slope for $M_{\text{gas}} \sim \text{SFR}$ should be close to the unit ($\text{Slope}_{M_{\text{gas}}-\text{SFR}} \sim 1$) with a clear explanation that the mean value of the $\text{Log } M_{\text{HI}} / M_{\text{H}_2}$ ratio is approximately constant $\sim 0.75 \pm 0.065$ for extragalactic CO survey spirals. Consequently, the atomic gas-phase amount in our study of spirals is approximately 6 times greater than the molecular gaseous amount. The result of this statistical analysis is, in general, consistent with the results of [32, 27], however, it contrasts with Young and Knezek's [33] conclusion that the quantities of molecules and phases of an atomic gas are equal. All molecular and atomic forms of cold interstellar hydrogen gas in extragalactic spirals depend greatly on the type of morphology.

We also revealed that the ratio ($L_{\text{FIR}}/L_{\text{B}} > 1/3$) for our spiral galaxies sample, which means the existence of spiral bar galaxies, undergoes bar-induced starbursts with illuminated blue optical and Far-infrared is approximate $\sim 10^{10} L_{\odot}$. The reason is thought to be the presence of a bar that activates the process of star formation in type spiral bar galaxies, this intimates that fuel availability is a factor that determines only galaxies that experience stellar explosions from bars, furthermore, our analysis confirms a good consensus with the literature [34]. Figure 4b (right panel/ dashed red line) exhibits the regression relationship between the ratio $L_{\text{FIR}}/L_{\text{B}}$ and the star formation rate increasing with a tendency toward linearity ($\text{Slope} \sim 1$), and our results of multiple regression analysis indicate there exists a significant correlation ($R \approx 0.6$) between these quantities. These extreme infrared luminosity galaxies are directly fuelled by massive starbursts, mainly dust-covered, at rates of star formation in the tens or yet hundreds M_{\odot}/yr , which can be concluded directly from L_{FIR} if the global relationship, $\text{SFR}_{\text{FIR}} \approx 1.7 \times 10^{-10} L_{\text{FIR}}$. The well-related far-infrared to blue optical-luminosity ratio $L_{\text{FIR}}/L_{\text{B}}$ star formation indices are used to compare star formation behavior in galaxies. On a timescale of billions of years, the L_{B} blue optical luminosity is a tracker of past star formation, while FIR and radio communication at a luminosity of 6 cm are trackers of modern star formation on a timescale of millions of years.

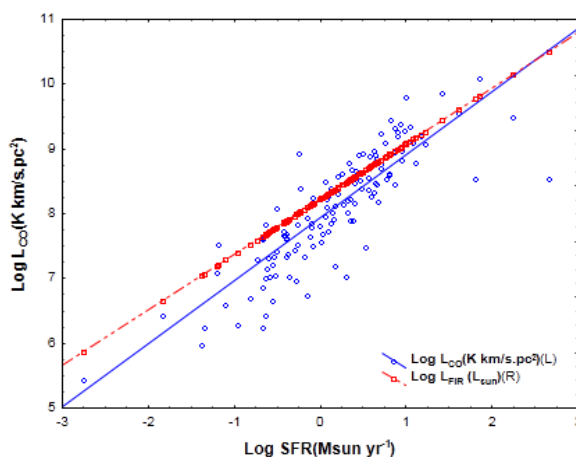


Figure 4 - (a) left panel- The relationship between L_{CO} , L_{FIR} and star formation rate (SFR) in scale logarithmic.

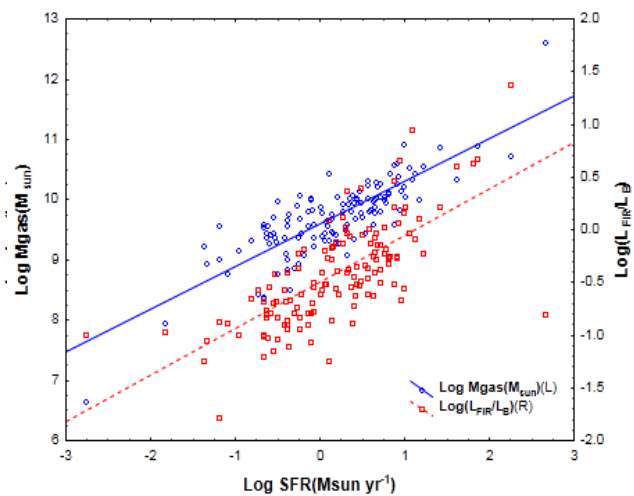


Figure 4 - (b) right panel- The total cold gas content M_{gas} and ratio $L_{\text{FIR}}/L_{\text{B}}$ as a function of (SFR).

5. Conclusion

As shown by the LFIR/LCO ratio computed from our results, these galaxies have exceptionally high lines of infrared detection at a factor twice as strong as the CO (J=1-0) line. We conclude that the contents of molecular hydrogen have a linear relationship with LCO. Based on our statistical analysis, we also found that the true meaning of the gas is revealed by the CO line emission spectra. CO observations are important for galaxies, particularly those with effective starbursts since it appears that molecular gas plays a role in the formation of stars. By calculating the rate of infrared luminosity (LFIR) to determine its effect on spiral galaxies, we realized that it emits distinctively from dust within molecular (CO) clouds in these galaxies, resulting in a high infrared luminosity. Our conclusions designate that thermal radio luminosity and LFIR are well associated with the CO line luminosity. The results indicate that the dust components contain a plurality of cold dust and a plurality of warm dust.

We've seen that L_{CO} and M_{H_2} have a very strong linear relation, with the slope of $\text{Log } L_{CO} - \text{Log } M_{H_2}$ equivalent to 1, and a very steep correlation coefficient ($R_{CO-MH_2}=1$). Due to the molecular gas's effectiveness in the M_{H_2} regions, the very high linear interaction potential between L_{CO} and M_{H_2} distinct in these types of galaxies suggests that the molecular gas is more abundant owing to its broad diffusion. Eventually, the work concluded the relationship slopes of L_{CO} -SFR and L_{FIR} -SFR are nearly linear 1, with a high partial correlation $R_{CO-SFR} \sim 0.73$ between L_{CO} -SFR and a significant correlation $R_{FIR-SFR} \sim 0.5$ between L_{FIR} -SFR. There should be very significant relationships between the amount of molecular gas CO and star formation indicator higher than the amount of far-infrared emission and spiral galaxies' SFR on all scales. For instance, a portion of the FIR radiation in some spiral galaxies can occur in the distributed atomic layer, making it insignificant to star formation regimes. We also remarked that the ratio ($L_{FIR} / L_B > 0.3$) of our extragalactic spirals sample, indicating the presence of spiral galaxies bar showing bar induced by stellar explosions with optical - blue and far-infrared illumination is approximate $\sim 10^{10} L_{\odot}$.

References

- [1] Bernard F. Burke, Francis G.-S. and Peter N. W., An introduction to Radio Astronomy, Fourth edition, Cambridge University Press, United Kingdom, 2019 ,p.345.
- [2] Alain O., "Molecules in galaxies", *Reports on Progress in Physics*, vol.70, Issue7, pp.1099-1176, 2007.
- [3] Sanders, D. B. et al, "Luminous Infrared Galaxies", *Astronomy and Astrophysics*, vol. 34, pp.749-792, 1996.
- [4] Ewen, H.I., & Purcell, E.M., "Observation of a Line in the Galactic Radio Spectrum: Radiation from Galactic Hydrogen at 1,420 Mc./sec", *Nature*, vol.168, Issue 4270, pp. 356, 1951.
- [5] Lavezzi T.E, and Dickey J.M., "Observations of (J=1-0) ^{12}CO in 44 cluster galaxies", *The Astronomical Journal*, vol.115, pp. 405-417, 1998.
- [6] Boselli A., Gavazzi G., et al., "Spectrophotometry of galaxies in the Virgo Cluster. I.The Star Formation History", *A. & A.*, vol.576, pp.576- 135, 2002.
- [7] Ralph J. D., Uli K. and Paolo S., "Baryons in Dark Matter Halos", *arXiv:astro-ph/0502215*, 2004.
- [8] Gao, Yu. and Solomon, P. M., "The Star Formation Rate and Dense Molecular Gas in Galaxies", *Astronomical*, vol. 606, pp.606 -271, 2004.
- [9] Jogee et al, "The Central Region of Barred Galaxies: Molecular Environment, Starbursts, and Secular Evolution", *Astrophysical Journal*, vol. 630, pp. 630- 837, 2005.
- [10] Al Najm M. N., "Studying the Atomic and Molecular Hydrogen Mass (MHI, M_{H_2}) Properties of the Extragalactic Spectra", *Iraqi Journal of Science*, vol. 61, pp. 1233-1243, 2020.
- [11] Frances V., "Catalog of CO Observations of Galaxies", *Astrophysical*, vol. 57, pp. 261-285, 1985.

- [12] Braine, J., Combes, F., Casoli, F. et al, "A CO(1-0) and CO(2-1) survey of nearby spiral galaxies. I. Data and observations", *Astronomy and Astrophysics*, vol. 97, pp.887-936, 1993.
- [13] Albrecht M. , Krügel E., and Chini R. , "Dust and CO emission towards the centers of normal galaxies, starburst galaxies, and active galactic nuclei", *A. &A.*, vol. 462, pp.575–579, 2007.
- [14] Yoshiaki S., "Galactic Radio Astronomy", *Springer Nature Singapore Pte Ltd*, p.17. 2017
- [15] Combes F., G.- B. S., Braine J., et al., "Galaxy evolution and star formation efficiency at $0.2 < z < 0.6$ ", *A.&A.*, vol. 528, A124, 2011.
- [16] Solomon P. M. & Vanden B. P. A., "Molecular Gas at High Redshift", *Annual Review of Astronomy and Astrophysics*, vol. 43, pp.677-725, 2005.
- [17] Lavezzi T. E., Dickey J. M., Fabienne C., et al., "A dual-Transition survey of co in the Coma cluster of galaxies", *Astronomical*, vol. 117, pp.1995-2009. 1999.
- [18] Aprajita V., Michael R.-R., Richard Mc M., and Andreas E., "Observations of hyper luminous infrared galaxies with the Infrared Space Observatory: implications for the origin of their extreme luminosities", *Mon. Not. R. Astron. Soc.*, vol. 335, pp. 574–592, 2002.
- [19] Orellana G., Nagar, N. M. et al. , "Molecular gas, dust, and star formation in galaxies I. Dust properties and scalings in 1600 nearby galaxies", *Astronomy & Astrophysics*, vol. 602, A68, 2017.
- [20] Martin, J. M., Bottinelli, L., Dennefeld, M., Gouguenheim, L., "An 18-cm OH and 21-cm HI survey of luminous far-infrared galaxies. II. HI properties", *Astronomy and Astrophysics*, vol. 245, pp. 393-417, 1991.
- [21] Dusan K., Yun Min S., and Young J. S., "CO Luminosity Functions For Far-Infrared– and B-Band–Selected Galaxies And The First Estimate For HI+H₂", *Astrophysical*, vol. 582, pp.659–667, 2003.
- [22] Yun Min S., Reddy N. A. and Condon J. J. , "Radio Properties of Infrared-Selected Galaxies in the IRAS 2 Jy sample", *Astrophysical*, vol. 554, pp. 803-822, 2001.
- [23] Lavezzi T. E. and Dickey J. M., "Observations OF ¹²CO (J=1-0) In 44 Cluster Galaxies", *Astronomical*, vol. 115, pp. 405-417, 1998.
- [24] Obreschkow D. and Rawlings S., "Understanding the H₂/H I ratio in galaxies", *Monthly Notices of the Royal Astronomical Society*, vol. 394, pp. 1857–1874, 2009.
- [25] Paturel, G. Thoreau G., Bottinelli L., et al., " Hyperleda II. The homogenized HI data", *A.&A.*, vol.412, pp.57–67, 2003.
- [26] Kandalyan R. A. , "The cold gas properties of Markarian galaxies", *A.&A.*, vol. 398, pp. 493–499, 2003.
- [27] Casoli, F. Dickey, J., Kazes, I., Boselli, A., "HI, H₂ and star formation in spiral galaxies in the region of the Coma supercluster", *Astronomy and Astrophysics*, vol. 309, pp. 43-58, 1996.
- [28] Tutti, Yoshinori, Sofue, Yoshiaki, Honma, et al., "CO Observations of Luminous IR Galaxies at Intermediate Redshift", *Astronomical*, vol. 52, pp.803-820, 2000.
- [29] Evans A. S., Mazzarella J. M., Surace J. A., et al. , "Molecular Gas and Nuclear Activity in Radio Galaxies Detected by IRAS", *Astrophysical*, vol. 159, pp. 197–213, 2005.
- [30] Boselli A., Cortese L., Boquien M., et al., " Cold gas properties of the Herschel Reference Survey II. Molecular and total gas scaling relations", *A.&A.*, vol. 564, A66, 2014.
- [31] Rashed, Y. E., Al Najm, M. N., and Al Dahlaki, H. H., "Studying the Flux Density of Bright Active Galaxies at Different Spectral Bands", *Baghdad Science Journal*, vol. 16, pp.230-236, 2019.
- [32] Kandalyan R. A., AL-Naimiy H.M.K., and Khassawneh A.M., "Star Formation Properties of Spiral Galaxies", *Astrophysics and Space Science*, vol.273, pp. 103–115, 2000.
- [33] Young, J.S. and Knezek, P.M., "The Ratio of Molecular to Atomic Gas in Spiral Galaxies as a Function of Morphological Type", *Astrophys. J.*, vol. 347, L55, 1989.
- [34] Huang, J.H., Gu, Q.S., Su, H.J., Hawarden, T.G., Liao, X.H. and Wu, G.X., "The bar-enhanced star-formation activities in spiral galaxies", *Astron. & Astrophys.*, vol.313, pp.13-24, 1996.

Table 1- Obtaining data for the parameters adopted in our study from works of literature [11,12 &13], NASA/IPAC Extragalactic archive (NED), and Lyon-Meudon Extragalactic Database website (hyperLeda).

NO.	NAME GALAXIES	TYPE TELESCOPE	$I_{co}(1-0)$ K KM/S	Θ_{HPBW} (ARCSEC)	REFERENCES OF COLLECTED DATA FROM COLUMNS 2 TO 4	M_{21}	M_{BT}	Z	F12 (JY)	F25 (JY)	F60 (JY)	F100 (JY)	F1.4 (JY)	F_{60} (MJY)	MORPHOLOGICAL TYPE
1.	NGC 157	NAR O	8	65	11	13.3	10.4	0.00551	1.61	2.17	17.93	42.43	0.1366	57	SAB(rs)bc
2.	NGC 253	NAR O	8.4	102	11	10.35	6.62	0.00081	41.04	154.67	967.81	1288.15	2.9947	2433	SAB(s)c
3.	NGC 520	NAR O	21.2	45	11	14.56	11.67	0.00761	1.07	3.08	31.62	47.76	0.1769	126	Sa
4.	NGC 613	NAR O	18	65	11	13.68	10.51	0.00494	2.25	4.32	27.38	59.21	0.1796	101	SB(rs)bc
5.	NGC 660	NAR O	14	65	11	12.44	11.26	0.00283	3.05	7.3	65.52	114.74	0.3738	184	SB(s)a
6.	NGC 992	NAR O	6.5	45	11	14.64	14.64	0.01381	0.56	1.76	11.4	16.72	0.0823	39	S
7.	NGC 1058	BTL	0.77	102	11	13.08	11.24	0.00173	0.225	0.1676	2.647	8.738	0.0069		SA(rs)c
8.	NGC 1068	NAR O	51	65	11	13.91	9.47	0.00379	39.84	87.57	196.37	257.37	4.85	2039	RSA(rs)b
9.	NGC 1097	NAR O	10	65	11	12.48	9.69	0.00424	4.16	9.27	58.29	114.82	0.413	126	SB(s)b
10.	NGC 1961	BTL	7	102	11	13.22	10.97	0.01312	0.9	0.99	7.17	23.37	0.1771	57	SAB(rs)c
11.	NGC 2403	NAR O	4.4	65	11	10.22	8.13	0.00044	3.34	6.29	51.55	48.49	0.33	46	SAB(s)cd
12.	NGC 2623	NAR O	4.8	65	11	16.69	13.06	0.01851	0.21	1.81	23.74	25.88	0.0962	59	Sb
13.	NGC 2903	NAR O	24	65	11	11.99	8.83	0.00183	5	7.64	52.38	47.36	0.4483	118	SAB(rs)bc
14.	NGC 3227	NAR O	4.4	65	11	14.26	11.1	0.00386	1.11	2.04	9.01	19.11	0.1007	44	SAB(s)a pec
15.	NGC 3504	NAR O	15	65	11	15.65	11.44	0.00509	1.11	4.03	21.43	34.05	0.2752	115	RSAB(s)ab
16.	NGC 3628	NAR O	27	65	11	11.88	9.15	0.00281	3.13	4.85	54.8	105.76	291.7	276	Sb/pec
17.	NGC 3642	BTL	0.82	102	11	13.12	11.54	0.0053	0.1272	0.09902	1.436	4.577	0.0343		SA(r)b c
18.	NGC 3690	NAR O	3.1	45	11		11.41	0.01041	3.9	24.14	121.64	122.45	0.6781	398	Sm
19.	NGC 4051	NAR O	3.9	65	11	13.67	10.44	0.00234	1.35	2.2	10.53	24.93	0.0981	31	SAB(rs)bc
20.	NGC 4102	NAR O	9.2	65	11	15.01	11.62	0.00282	1.77	6.83	46.85	70.29	0.2734	70	SAB(s)b
21.	NGC 4237	FCRA O	2.3	45	11	16.1	11.95	0.00289	0.2693	0.321	2.764	9.189	0.0077		SAB(rs)bc
22.	NGC 4254	FCRA O	17.6	45	11	12.71	10.17	0.00803	3.67	4.38	37.46	91.86	0.439	108	SA(s)c
23.	NGC 4293	FCRA O	4.4	45	11	17.66	10.76	0.00298	0.24	0.64	3.86	7.72	0.0193	11	RSB(s)0/a
24.	NGC 4303	NAR O	7	65	11	12.82	10.02	0.00522	3.28	4.9	37.27	78.74	0.4358	178	SAB(rs)bc
25.	NGC 4388	FCRA O	2.9	45	11	15.35	10.77	0.00842	1.01	3.57	10.27	17.15	0.1204	93	SA(s)b
26.	NGC 4438	FCRA O	4.2	45	11	15.09	10.61	0.00024	0.2089	0.1743	3.761	11.27	0.0642	70	SA(s)0/a pec
27.	NGC 4501	FCRA O	15.4	45	11	13.82	9.62	0.00761	2.29	2.98	19.68	62.97	0.277	85	SA(rs)b
28.	NGC 4527	BTL	15.5	102	11	12.88	10.37	0.00579	2.65	3.55	31.4	65.68	0.178	151	SAB(s)bc

29.	NGC 4535	FCRA O	5.4	45	11	12.91	10.41	0.00655	1.04	1.34	11.45	32.52	0.106	38	SAB(s) jc
30.	NGC 4571	FCRA O	2	45	11	14.94	11.66	0.00114	0.1221		1.096	5.782	0.005		SA (r)d
31.	NGC 4631	NAR O	9	65	11	11.04	7.99	0.00202	6.81	11.24	99.69	193.26	448.6	438	SB(s)d
32.	NGC 4654	FCRA O	9.8	45	11	13.16	10.48	0.00349	1.01	1.73	13.39	37.77	0.123	44	SAB(r) s)cd
33.	NGC 4698	FCRA O	1.7	45	11	13.73	10.95	0.00337			0.2579	1.864	0.002		SA(s)a b
34.	NGC 4736	NAR O	4.6	65	11	13.39	8.54	0.00103	5.07	6.11	71.54	120.69	0.00889	117	RSA(r) ab
35.	NGC 4826	NAR O	12	65	11	13.39	8.71	0.00136	1.71	2	33.86	77.38	0.1011	56	RSA(r) s)ab
36.	NGC 4868	BTL	0.98	102	11	16.21	12.78	0.01556	0.2341	0.4239	3.238	8.552	0.0276		SAb
37.	NGC 5194	NAR O	3	65	11	12.16	8.34	0.00154	7.21	9.56	97.42	221.21	0.4303	436	SA(s)b c pec
38.	NGC 5248	NAR O	19	65	11	12.94	10.39	0.00384	1.75	3.02	20.91	53.48	0.1603	68	SAB(r) s)bc
39.	NGC 5457	NAR O	2	65	11	10.41	8.29	0.0008	6.2	11.78	88.04	52.84	0.75	150	SAB(r) s)cd
40.	NGC 5921	BTL	1.86	102	11	13.94	11.22	0.00494	0.2088	0.2488	2.912	10.21	0.0242		SB (r)bc
41.	NGC 6240	NAR O	9.8	65	11	16.14	13.26	0.02448	0.59	3.55	22.94	26.49	0.4272	179	S0-a
42.	NGC 6412	BTL	0.45	102	11	14.24	12.08	0.00438	0.29	0.25	2.71	7.78	0.0249		SA(s)c
43.	NGC 6500	NAR O	3.9	65	11	14.66	12.49	0.01002	0.1007	0.1005	0.6424	2.548	0.1829	176	SAab
44.	NGC 6814	NAR O	2.5	45	11	13.84	10.35	0.00521	0.92	1.04	6.53	19.67	0.0519		SAB(r) s)bc
45.	NGC 6951	NAR O	6	65	11	13.94	10.05	0.00475	1.34	2.16	16.24	41.77	0.0704	32	SAB(r) s)bc
46.	NGC 7371	BTL	0.8	102	11	14.09	12.36	0.00895							RSA (r)0/a
47.	NGC 7674	NAR O	4.1	65	11	15.31	13.59	0.02892	0.68	1.92	5.36	8.33	0.2214	86	SA (r)bc pec
48.	NGC 7742	BTL	1.5	102	11	15.08	12.01	0.00555	0.2	0.38	2.79	7.11	0.0272		SA (r)b
49.	NGC 7793	NAR O	3	65	11	11.88	9.19	0.00077	1.32	1.67	18.14	54.07	0.103		SA(s)d m
50.	IC 342	BTL	1.1	102	11	8.03	6.14		14.92	34.48	180.8	391.66	0.1919	124	SAB(r) s)cd
51.	IC 4553	BTL	1.8	102	11	14.24	13.38	0.01813	0.61	8	104.09	115.29	0.3268	204	Sm
52.	ESO 056- G 115	AAT	15	228	11	2.71	0.41	0.00093	2781.9	7824.19	82917	184686.7	426		SB(s) m
53.	UGC 8965	BTL	0.32	102	11	17.54	15.5	0.00681							Sd
54.	IC 750	IRAM	58	23	12	14.19	12.33	0.00234					0.1267	50	SAb
55.	NGC 278	IRAM	18	23	12	13.4	10.85	0.00209	1.65	2.65	25.03	44.46	0.1422	63	SABb
56.	NGC 628	IRAM	4.1	23	12	11.56	9.35	0.00219	2.45	2.87	21.54	54.45	0.173	34	Sc
57.	NGC 0864	IRAM	6	23	12	12.9	11.13	0.00521	0.56	0.32	4.31	10.02	0.0297		SABc
58.	NGC 0891	IRAM	96	23	12	12.13	9.7	0.00176	5.27	7	66.46	172.23	0.2422	342	Sb
59.	NGC 0925	IRAM	1.9	23	12	11.76	9.77	0.00185	0.26	0.66	7.65	26.68	0.0109	462	Scd
60.	NGC 1042	IRAM	2.9	23	12	13.44	11.05	0.00457	0.1003	0.2207	1.57	5.889			SABc
61.	NGC 1055	IRAM	46	23	12	12.59	10.84	0.00331	2.24	2.84	23.37	65.26	0.2009	63	SBb
62.	NGC 1084	IRAM	31	23	12	13.31	10.76	0.00469	1.96	3.2	29.41	58.64	0.315	121	Sc
63.	NGC 1087	IRAM	15	23	12	14.08	10.98	0.00506	0.97	1.41	12.16	27.98	0.136	45	Sc

64.	NGC 1637	IRAM	13	23	12	13.16	11.27	0.00239	0.65	1.47	6.61	15.71	0.0166		Sc
65.	NGC 2146	IRAM	118	23	12	13.23	9.99	0.00298	7.36	21.66	154.12	217.44	1.0745		SBab
66.	NGC 2681	IRAM	30	23	12	18.38	11.04	0.00231	0.43	0.58	7.14	11.22	0.0102		S0-a
67.	NGC 2715	IRAM	7.6	23	12	13.74	11.12	0.00447	0.1822	0.169	1.839	10.16	0.0272		SABc
68.	NGC 2820	IRAM	9.8	23	12	13.43	11.36	0.00525	0.2001	0.2515	4.34	10.3	0.0481		SBc
69.	NGC 2841	IRAM	6	23	12	12.19	9.54	0.00213	0.9	0.83	4.41	24.21	0.0359	33	SBb
70.	NGC 2964	IRAM	25	23	12	14.35	11.75	0.00443	0.82	1.92	12.07	25.42	0.1066	32	SBc
71.	NGC 2985	IRAM	12	23	12	12.97	10.96	0.00441	0.9	0.86	6.31	21.28	0.0441		SAb
72.	NGC 3079	IRAM	212	23	12	12.77	9.97	0.00372	2.54	3.61	50.67	104.69	0.7707	327	SBc
73.	NGC 3187	IRAM	3.5	23	12	15.09	12.84	0.00527					0.0026		SBc
74.	NGC 3198	IRAM	11	23	12	12.17	9.94	0.0022	0.71	1.08	7.15	18.44	0.0384		Sc
75.	NGC 3310	IRAM	3.6	23	12	13.29	11.15	0.00331	1.54	5.32	34.56	44.19	0.3642	149	SABb
76.	NGC 3344	IRAM	4.3	23	12	12.2	10.32	0.00194	1.04	1.42	9.9	29.21	0.0802	27	SBc
77.	NGC 3351	IRAM	17	23	12	13.5	10.14	0.0026	1.04	2.79	19.66	41.1	0.0436		Sb
78.	NGC 3359	IRAM	3	23	12	12.27	10.75	0.00338	0.43	0.61	6.61	17.38	0.0391		Sc
79.	NGC 3368	IRAM	35	23	12	12.99	9.74	0.00299	0.98	0.51	10.51	31.63	0.0316		SAb
80.	NGC 3486	IRAM	7	23	12	12.57	10.72	0.00227	0.62	0.24	6.26	16.42	0.0547	57	Sc
81.	NGC 3627	IRAM	90	23	12	13.37	9.09	0.00243	4.82	8.55	66.31	136.56	0.46	141	Sb
82.	NGC 3810	IRAM	12	23	12	13.59	10.8	0.00331	1.46	1.62	13.63	35.07	0.1279	46	Sc
83.	NGC 4274	IRAM	10	23	12	15.2	10.86	0.0031	0.3119	0.4288	4.352	13.28	0.00125		SBab
84.	NGC 4314	IRAM	24	23	12		11.28	0.00321	0.165	0.3617	3.788	7.14	0.0141		Sa
85.	NGC 4321	IRAM	78	23	12	13.16	9.83	0.00524	2.52	3.1	26	68.37	0.0871	90	SABb
86.	NGC 4414	IRAM	57	23	12	13.24	10.49	0.00239	2.78	3.61	29.55	70.69	0.2422	78	Sc
87.	NGC 4565	IRAM	12	23	12	11.34	8.97	0.0041	1.36	1.36	7.79	34.62	0.0583	2.5	Sb
88.	NGC 4651	IRAM	6	23	12	13.27	10.95	0.00263	0.47	0.66	5.94	16.56	0.0352	700	Sc
89.	NGC 5005	IRAM	76	23	12	14.53	9.7	0.00316	1.65	2.26	22.18	63.4	0.1827	62	SABb
90.	NGC 5033	IRAM	21	23	12	12.29	10.08	0.00292	1.77	2.14	16.2	50.23	0.1228	82	Sc
91.	NGC 5112	IRAM	1.7	23	12	13.63	12.2	0.00325		0.1796	1.863	6.049	0.0173		SBc
92.	NGC 5364	IRAM	5	23	12	13.09	10.5	0.00414		0.1897	2.273	12.05	0.0113		SBc
93.	NGC 5907	IRAM	32	23	12	11.99	9.71	0.00222	1.29	1.44	9.14	37.43	0.167	35	SABc
94.	NGC 6015	IRAM	5.1	23	12	13.01	10.93	0.00276	0.6	0.7	4.42	13.74	0.0201		Sc
95.	NGC 6217	IRAM	19	23	12	13.36	11.46	0.00454	0.74	2.03	11.35	20.62	0.0808		SBc
96.	NGC 6384	IRAM	7.6	23	12	13.12	10.55	0.00555	0.1881	0.1908	2.287	13.07	0.0174		SBc
97.	NGC 7217	IRAM	10	23	12	14.97	10.54	0.00318	0.63	0.68	6.1	20.91	0.0178		SAb
98.	NGC 7331	IRAM	38	23	12	12.08	9.19	0.00272	3.94	5.92	45	110.16	0.329	96	SBc
99.	NGC 7640	IRAM	2.3	23	12	11.76	9.99	0.00123	0.16		3.7	11.45	0.0168		Sc

100.	NGC 7741	IRAM	1.1	23	12	13.48	11.16	0.0025		0.2265	2.274	6.984	0.0184		SBc
101.	NGC 0834	MRT	28.1	24	13	15.77	13.14	0.01532	0.41	0.84	6.65	12.77	0.0621		Sb
102.	NGC 0877	MRT	12.2	24	13	14.02	11.82	0.01305	1.14	1.94	11.82	25.56	0.1099	38	SABc
103.	NGC 0935	MRT	12.4	24	13	14.62	12.6	0.01382	0.2606	0.2881	3.138	9.528	0.0551		Sc
104.	NGC 1134	MRT	41.6	24	13	13.6	11.75	0.01214	0.55	0.92	9.09	16.43	0.155	32	Sb
105.	UGC 02627	MRT	2.7	24	13	14.67	12.97	0.01409	0.2434	0.2961	3.105	9.114	0.0216		Sc
106.	UGC 02936	MRT	36	24	13	14.95	12.08	0.01272	0.29	0.49	4.65	11.15	0.0374		Sc
107.	ESO 118-G16	SEST	4.6	45	13	15.43	12.23	0.00378	0.49	0.76	6.06	12.67		12.9	SBc
108.	NGC 2339	MRT	47.2	24	13	14.2	11.77	0.00736	0.59	2.4	17.6	31.82	0.1086	34	SBc
109.	ESO 492-G2	SEST	4.6	45	13	13.38	11.63	0.00864	0.41	0.79	7.94	14.88	0.1014		Sb
110.	NGC 2276	MRT	18	24	13	14.29	11.36	0.00806	1.48	2.23	14.15	31.58	0.2692		SABc
111.	NGC 2397	SEST	14.4	45	13	14.92	11.09	0.00455	0.73	1.08	8.48	19.18			SBb
112.	ESO 493-G16	SEST	21.9	45	13	12.41	12.69	0.00884	0.826	1.325			0.1183		SBc
113.	NGC 2640	SEST	4.2	45	13		10.77	0.00351	0.32	0.4	4.27	11.43		43	E-S0
114.	ESO 563-G28	SEST	9.8	45	13	15.61	12.53	0.00872	0.36	0.81	8.21	15.84	0.0616		SBab
115.	NGC 2706	SEST	6	45	13	15.41	12.91	0.00544	0.56	0.59	6.64	14.01	0.0529	18.9	SBc
116.	NGC 2967	SEST	9.3	45	13	13.46	11.79	0.00632	0.64	1.09	5.69	14.48	0.155	49	Sc
117.	ESO 500-G34	SEST	4.4	45	13	15.98	13.99	0.01222	0.38	1.43	10.46	16.01	0.0578		S0-a
118.	ESO 317-G23	SEST	9.5	45	13		13.16	0.00965	0.34	0.89	13.83	23.08	0.0757		Sa
119.	NGC 3278	SEST	5.9	45	13	15.64	12.45	0.00988	0.59	0.91	7.1	14.66	0.0617		Sc
120.	NGC 3366	SEST	5	45	13	14.39	11.02	0.00965		0.1782	3.252	10.27			SBb
121.	ESO 093-G03	SEST	4.3	45	13	13.3	12.15	0.00611	0.67	1	10.05	17.89		35	S0-a
122.	NGC 3655	SEST	9.9	45	13	14.79	11.93	0.00491	0.65	1.12	8.48	19.75	0.0672		Sc
123.	NGC 3800	MRT	20	24	13	15.79	12.2	0.01105					0.0501		SABb
124.	NGC 3882	SEST	7.8	45	13	13.86	10.54	0.00611	1.51	2.67	19.84	37.38		95	SBbc
125.	NGC 3987	MRT	37.3	24	13	15.14	12.97	0.01502	0.2108	0.343	4.776	15.06	0.0576		SBb
126.	NGC 4746	SEST	4.6	45	13	14.59	12.24	0.00595	0.3782	0.5178	4.98	12.24	0.0556		Sb
127.	NGC 4808	MRT	11.3	24	13	13.02	11.53	0.00253	0.62	0.74	6.92	16.05	0.0624		SABc
128.	NGC 4900	MRT	7.3	24	13	14.49	11.75	0.0032	0.49	0.76	5.97	13.96	0.0467		Sc
129.	NGC 5156	SEST	8	45	13	14.38	11.79	0.00997	0.2954	0.445	4.132	10.41			SBb
130.	NGC 5600	SEST	4.9	45	13	15.42	12.8	0.00773	0.35	0.72	5.44	11.68	0.0383		SABc
131.	ESO 272-G14	SEST	11.5	45	13	14.49	11.21	0.00654	1.4	2.33	19.13	38.07	0.189	100	SABb

132.	ESO 272- G23	SEST	4.3	45	13	14. 45	12.2 2	0.00 956	0.25 8	0.35 98	4.07 9	10.7 3			Sc
133.	NGC 5719	MRT	42.6	24	13	13. 65	12.7 1	0.00 578	0.52	1.09	8.61	17.9 6	0.05 87		SABa
134.	ESO 223- G12	SEST	5.9	45	13	13. 71	11.1 2	0.00 483		0.33 1	4.43 6				SBc
135.	NGC 6215	SEST	10	45	13	13. 05	11.0 8	0.00 522	1.94	3.53	29.9 7	47.5 5	0.05 4	110	Sc
136.	ESO 282- G03	SEST	7.2	45	13	14. 5	11.9 5	0.01 695	0.23 57	0.33 42	3.34 4	9.91 7			Sc
137.	NGC 6753	SEST	13.9	45	13	14. 45	11.5	0.01 057	0.94	0.98	9.79	27.1 4		35	Sb
138.	ESO 467- G27	SEST	7.1	45	13	14. 71	12.7 8	0.01 74	0.44	0.58	5.58	12.4 8	0.05 24		SABb
139.	ESO 346- G22	SEST	1.7	45	13	14. 22	12.1 7	0.00 431	0.17 8	0.46 33	4.13 1	11.2 9			SBc
140.	NGC 7448	SEST	5.9	45	13	14. 02	11.1 6	0.00 732	0.45	0.77	8.88	17.8 9	0.08 34		Sc